

Figure 2: Theoretical equilibrium binary phase diagram Al-Cu, calculated by ThermoCalc¹ (TCBin database)
Slika 2: Teoretični ravnotežni binarni fazni diagram Al-Cu, izdelan s ThermoCalc-om¹ (podatkovna baza TCBin)

Al, Mg and Si have a large affinity for oxygen ($\Delta G_f = -277.8$ kJ/mol at the melting point of Al). Therefore, some surface oxidation and a thin Al_2O_3 film is formed during the alloy synthesis if a very pure protective atmosphere (Ar or N_2) is not used. Some complex inclusions containing Al_2O_3 , MgO and SiO_2 can also be formed.

For this type of alloy there is a typical dendrite morphology of solidification during the cooling and casting into a sand, metal or graphite mold at normal cooling rates (0.1 K/s to 100 K/s). The measure for cooling rate and segregation is the so-called Secondary Dendrite Arm Spacing (SDAS). It generally follows exponent law, $\lambda = k \cdot \nu^{-n}$; i.e., the larger is the cooling rate ν , the finer are the dendrites and the smaller is the space between the secondary dendrite arms λ , as well as the alloy being more micro homogeneous over its volume. Some theoretical models exist^{5,6} for a determination of λ , and recently some researchers have also tried to predict λ with ANNs (Artificial Neuron Networks)⁷. For Al alloys different values for the

alloy-dependent parameter k (approx. 110) and exponent n (approx. 0.30) are reported. Generally, the parameter k depends on the chemical composition; i.e., decreasing with an increasing concentration of alloying elements.

Figure 3 shows an example of the secondary dendrite arm spacing λ vs. cooling rate ν diagram for the selected values of $k \approx 109$ and $n \approx 0.33$. One can clearly see that for the selected parameters λ decreases from approximately 500 μm at cooling rate $\nu = 0.01$ °C/s, over 110 μm at $\nu = 1$ °C/s, and finally at $\nu = 100$ °C/s it is only approximately 24 μm .

The physical and mechanical properties of metal-based alloys are dependent on the chemical composition (alloying and trace elements) and the microstructure controlled by the solidification rate connected with the type and geometry of the mold and product, respectively. A higher initial solidification rate (cooling rate in the mushy zone) produces a finer dendrite morphology of solidification, a smaller segregation of alloying elements, as well as better mechanical properties (higher yield/tensile strength and hardness). The refinement of the microstructure also improves the ductility and toughness for a given strength level. Recently, new software⁶ has been developed for the relatively accurate prediction of the mechanical properties of Al alloys over a wide range of chemical compositions and solidification conditions.

Figure 4 shows the theoretical equilibrium thermodynamic phase stability of the model alloy with actual chemical composition determined at the Institute of Metals and Technology (IMT), Ljubljana Slovenia (Table 1). It is clear that in this case seven phases are stable in the temperature region between 20 °C and 700 °C. However, also in this system the main phases remain α -Al (fcc-Al solid solution), Al_2Cu and liquid L. The theoretical calculation predicts the existence of the pro-eutectic θ -phase (Al_2Cu) between 20 °C and 514 °C. The solid solution α -Al is stable up to 646.4 °C. In this case the autonomous one-phase region of the α -Al solid

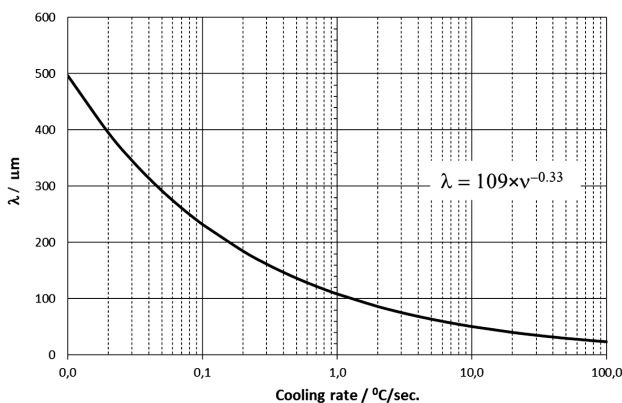


Figure 3: Prediction of the secondary dendrite arms space vs. cooling rate for the Al-based alloy and selected values of the alloy-dependent parameters

Slika 3: Napoved razdalje med sekundarnimi dendritnimi vejami v odvisnosti od hitrosti ohlajanja za zlitino na osnovi Al in izbrane zlitinske parametre

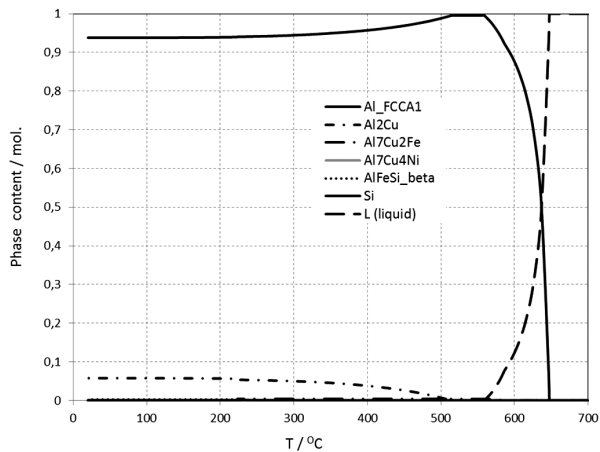


Figure 4: Theoretical equilibrium thermodynamic stability of the phases in the alloying system with the real chemical composition of the model alloy, calculated by ThermoCalc¹.

Slika 4: Teoretična ravnotežna termodinamska stabilnost faz v sistemu z dejansko kemijsko sestavo modelne zlitine, izračunana s ThermoCalc-om¹

solution does not exist, because the Fe-based intermetallic phase $\text{Al}_7\text{Cu}_2\text{Fe}$ is stable up to 579 °C. The optimal temperature interval for homogenization annealing is between 547 °C and 559 °C. But in this temperature region there is also a small content of $\text{Al}_7\text{Cu}_2\text{Fe}$. Only liquid is present above 646.4 °C. Silicon has a low solubility in the present alloy. Therefore, it appears in the temperature region between 20 °C and 223 °C as β -phase (AlFeSi) and between 223 °C and 340 °C as elementary crystals of Si, respectively. As already mentioned, in the temperature region between 223 °C and 579 °C, the intermetallic phase $\text{Al}_7\text{Cu}_2\text{Fe}$ is also stable, because of the presence of iron in the model alloy. Besides this, the presence of traces of Ni can stabilize the $\text{Al}_7\text{Cu}_4\text{Ni}$ phase in the temperature region between 20 °C and 548 °C. Some traces of Mg are also detected in the model alloy. In this case we can also expect the presence of the $\text{Al}_5\text{Cu}_2\text{Mg}_8\text{Si}_6$ intermetallic phase. However, it should be noted that the content of Ni and Mg in the model alloy is very low and these phases could be neglected.

2 EXPERIMENTAL

The model alloy Al-w(Cu) 4.5 %, was prepared in the frame of the project entitled "Advanced modelling and simulation of liquid-solid state processes"⁸. In the frame of this project the development of the microstructure during solidification in the mushy zone are studied on the macro and micro levels for the selected Al- and Fe-based complex alloys. The microscopic model is to be solved by the cellular automata concept.

2.1 Synthesis of the model alloy

The model alloy was synthesised in a graphite pot of a laboratory melting furnace 10 kW under an Ar protective atmosphere. The furnace is one of the basic compo-

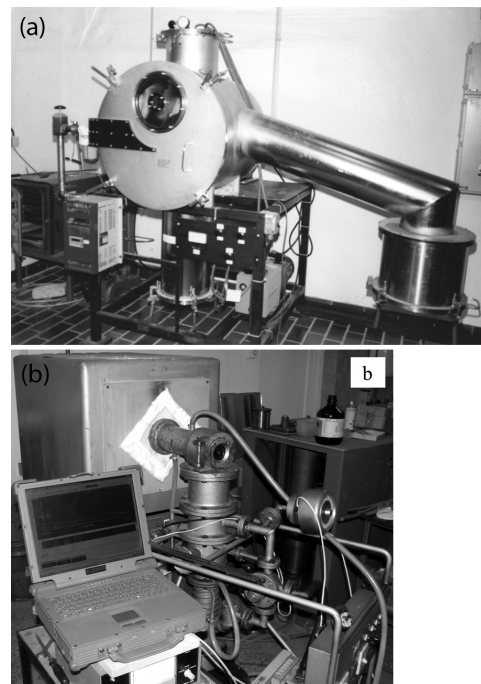


Figure 5: a) Chamber of melt-spinner with inductive melting furnace and b) laboratory tube furnace for heat treatment of the model alloy

Slika 5: a) Laboratorijska naprava Melt-Spinner z induktivno talilno pečico in b) laboratorijska cevna peč za toplotno obdelavo modelne zlitine

nents of the Melt-Spinner M-10 Marco Materials Inc. (**Figure 5a**) which serves primarily for the preparation of rapidly solidified ribbons with the casting of the melt on a rotating Cu-wheel.

As the basic raw materials for the preparation of the model alloy, commercially available materials of technical purity (Al 99.7 % of manufacturer Impol Slovenska Bistrica and commercial Cu 99.9 %) were used. Four batches of 200 g were prepared. Each weight was melted and then cooled under natural cooling conditions down to the room temperature. The chamber of the melt-spinner was evacuated with a rotary vacuum pump (absolute pressure approx. 10 Pa) and then filled with Ar (over pressure 60 kPa abs.) before melting. Individual weights were heated up in the inductive melting furnace to 800 °C in 20 min, homogenized for 10 min and then cooled down. The temperature was followed with a DataLogger and measured with a Pt-PtRh10 thermocouple, located in the middle of the graphite melting pot. It was protected against the melt by a ceramic (alumina) protective tube. The final bulk chemical composition of the prepared alloys was checked using a fast portable XRF (X-Ray Fluorescence) analyser XL3Thermo Fischer Scientific Niton and a more accurate classical ICP OES (Ion Coupled Plasma – Optical Emission Spectroscopy) Agilent 720 instrument with a lower limit of detection ($w < 0.001$ % of individual element). **Table 1** shows the results of both chemical analyses. Some impurities are detected because of the use of technically pure raw

materials. Besides Al and Cu, some Fe and Si, as well as traces of Ni, Zn and Mg, were detected.

Table 1: Average bulk chemical composition of prepared batches of model alloy in mass fractions, w/%

Tabela 1: Povprečna kemijska sestava izdelanih šarž modelnih zlitin v masnih deležih, w/%

Chemical composition	Cu	Si	Zn	Fe	Mg	Ni	Al
XRF	4.30	0.14	0.010	0.12	–	–	balance
ICP OES	4.45	0.14	0.002	0.09	$< 10^{-3}$	0.006	balance

Five cylinders of diameter 45 mm and height 40 mm weighing approximately 200 g were prepared in this way (**Figure 6**) for further experiments and microstructure investigations. The cylinders were cleaned of surface oxidation by smooth drilling. Further heat treatments of the cylinder were performed due to the formation of an appropriate microstructure at different cooling rates. It is very difficult to obtain the required cooling rate because the real cooling conditions vary over the cross-sections (volume) of relatively large samples, and they are not constant in different temperature regions. The laboratory equipment also does not enable the use of a larger number of thermocouples at different locations of the samples. It can be considered that below 200 °C significant microstructure changes do not happen in a relatively short period of time. Therefore, we can assess the average cooling rate above this temperature. However, in the literature⁶ one can find different approaches to cooling-rate definition (initial, average, for a given temperature interval etc.) depending on how it can influence the microstructure formation. During the planning of the present project we did not have in mind that for the formation of a selected Al-4.5 Cu binary alloy that the initial cooling rate and cooling rate in the mushy zone are important. Therefore, it was planned that three different characteristic average cooling rates will be obtained; i.e., very slow (< 0.1 °C/min or 0.0017 °C/s), natural cooling rate (30 °C/min to 40 °C/min or 0.5 °C/s to 0.7 °C/s) and very fast quenching (300–400 °C/min or

5.0 °C/s to 6.7 °C/s). Actually, the following experimental cooling rates are obtained:

Sample 0 to 4 – reference materials – only synthesised alloy (melted in graphite pot of inductive furnace and cooled down). **Figure 7** shows the temperature profile of the alloy synthesis, i.e., heating and cooling in a graphite melting pot. During cooling there is a clearly visible solidification interval between approximately 645 °C and 550 °C. This is in relatively good agreement with the theoretical prediction, which predicts that the solidification starts at 648 °C and ends at 564 °C (**Figure 4**). The obtained cooling rate between 645 °C and 100 °C is approximately 10 °C/min and approximately 0.17 °C/s, respectively. For the formation of the dendrite morphology of solidification the cooling rate in the mushy zone is important. This was assessed at approximately 30 °C/min and 0.5 °C/s, respectively. In this case, one can estimate from **Figure 3** the SDAS on 130 µm.

Samples 0 and 1 were retained in the original state for metallographic investigations. However, the samples 2, 3 and 4 were additionally heat treated in order to obtain the planned cooling rates. The samples were heated up to 610 °C into the mushy zone (semi-solid state) and then cooled down.

With sample 2 we tried to simulate natural cooling conditions in the tube furnace (**Figure 5b**). A half part of the cylinder was heated up to 610 °C for 10 min and then a ceramic tube was pulled from the heating chamber of the furnace. The obtained cooling rate in the temperature interval between 610 °C and 200 °C was approximately 12 °C/min (0.2 °C/s) and below 200 °C it was approximately 0.7 °C/min (0.012 °C/s) (**Figure 8**). The maximum cooling rate in the mushy zone was estimated to be approximately 0.4 °C/s ($SDAS \approx 138$ µm). But it has to be noted that the prepared alloy was not completely melted. As one can see the average cooling rate of the material is rather lower than planned 30–40 °C/min (0.5 – 0.7 °C/s) and similar to that obtained during the alloy synthesis.

Sample 3 was heated to 610 °C for 10 min and then fast cooled, i.e., quenched in water. The estimated aver-

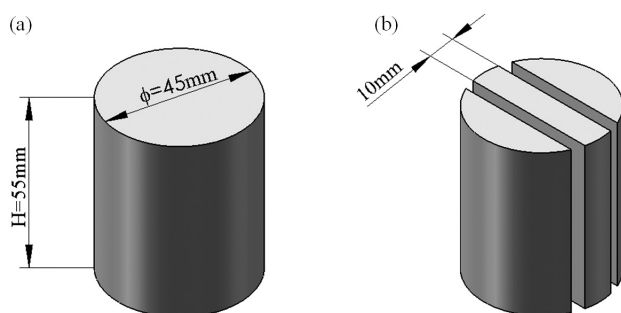


Figure 6: a) Schematic presentation of the cast cylinder of the model Al-w(Cu) 4.5 % alloy and a) its cutting into specimens for the preparation of metallographic samples

Slika 6: a) Shematični prikaz ulitka modelne zlitine Al-w(Cu) 4,5 % in b) njegov razrez za pripravo metalografskih vzorcev

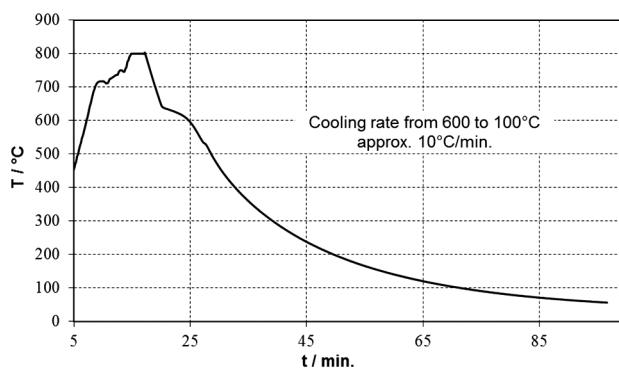


Figure 7: Temperature profile obtained during the synthesis of the model alloy Al-w(Cu) 4.5 %

Slika 7: Temperaturni profil sinteze vzorca modelne zlitine Al-w(Cu) 4,5 %

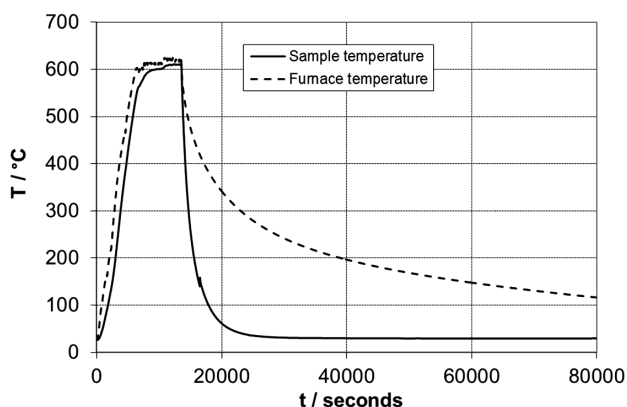


Figure 8: Heating/cooling diagram for model alloy Al-w(Cu) 4.5 % in the ceramic tube of the furnace, sample 2, ceramic tube with sample pulled from the furnace chamber

Slika 8: Diagram segrevanja in ohlajanja modelne zlitine Al-w(Cu) 4,5 % v cevi cevne peči (po segrevanju je cev potegnjena iz peči), vzorec 2

age cooling rate of this sample was 1220 °C/min (20.3 °C/s), which is rather faster than planned.

Sample 4 – with this sample we tried to simulate very slow cooling. The cylinder was cooled down from 610 °C over approximately 4 d with an approximate cooling rate of 0.1 °C/min, (0.002 °C/s) (**Figure 9**). In this case the maximum cooling rate was 0.7 °C/min and 0.01 °C/s, respectively (*SDAS* ≈ 500 μm).

From the above-described experiments we can conclude that the experimental work was not completely successful, as planned in the frame of the project. In spite of this the obtained results are very interesting and are published as follows.

2.2 Microstructure investigations of the model alloy

Cast and heat-treated cylinders of the model alloy Al-w(Cu) 4.5 % were cut up into slices and prepared for microstructure investigations (**Figure 10**). The metallographic specimens were prepared with Struers equipment

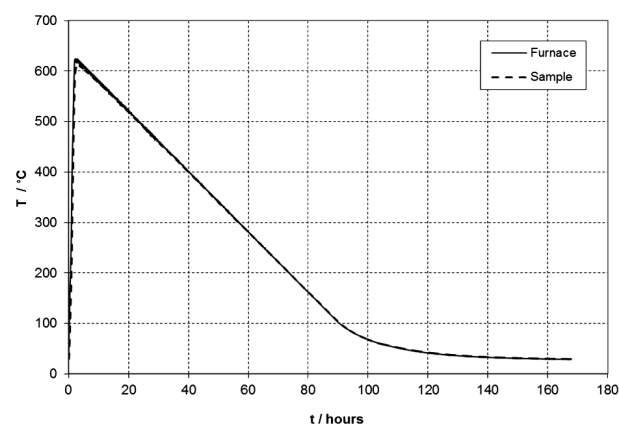


Figure 9: Diagram of heating and very slow cooling of sample 4 of model alloy Al-w(Cu) 4.5 % in tube furnace

Slika 9: Diagram segrevanja in zelo počasnega ohlajanja vzorca 4 modelne zlitine Al-w(Cu) 4,5 % v cevni peči

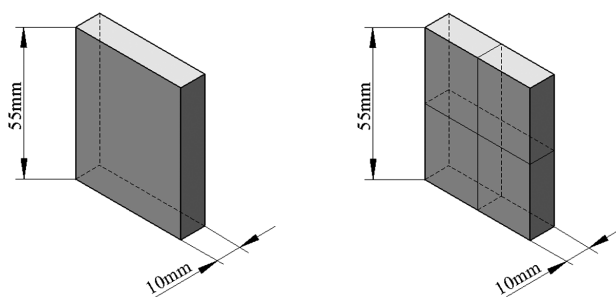


Figure 10: Schematic presentation of ingot cutting of the model alloy for the preparation of metallographic samples

Slika 10: Shematični prikaz razreza ingota modelne zlitine Al-w(Cu) 4,5 % za pripravo metalografskih obruskov

(electron saw Accutom 50, automatic press Pronto-Press-20 and grinding/polishing apparatus Abramin with MD-system). The microstructure characterization with a light (LM, Nikon Microphot FXA with 3CCD video camera Hitachi HV-C20AMP and software ANALYSIS PRO 3.1) and a scanning electron microscope (SEM; JEOL FE HR JSM-6500F) combined with micro-chemical analysis based on a measurement of the dispersed kinetic energy of X-rays (EDS – Energy Dispersive X-ray Spectrometer) on polished and etched metallographic plates 20 mm × 20 mm (specimens) were performed. A systematic non-continuous point profile (10-points per 20 μm) and surface (mapping) EDS analyses at different locations (**Figure 11**) of the samples were then performed.

3 RESULTS AND DISCUSSION

The prepared model alloys were cooled down with cooling rates between 0.002 °C/s and 20.3 °C/s. In all these cases one can expect a dendrite morphology of

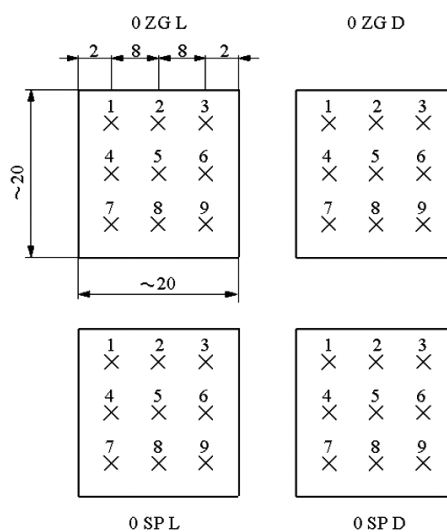


Figure 11: Schematic presentation of EDS analyses' locations on metallographic samples of the model alloy Al-w(Cu) 4.5 %

Slika 11: Shematični prikaz analiznih mest SEM/EDS na metalografskih obruskah modelne zlitine Al-w(Cu) 4,5 %

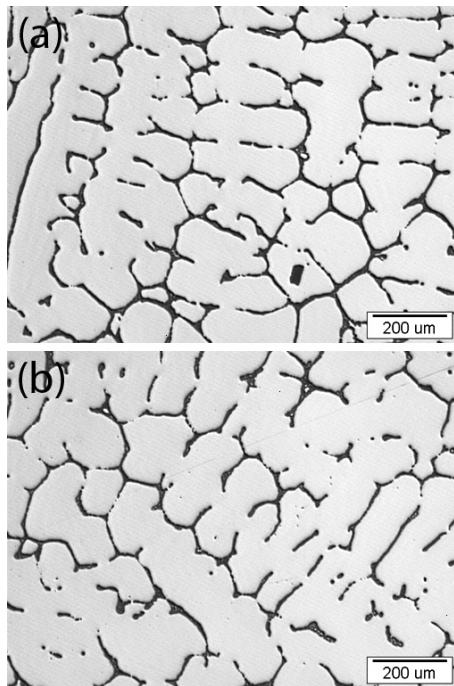


Figure 12: Microstructure of model alloy Al-w(Cu) 4.5 % visible under LM: a) sample 1, SDAS = 83 μm and b) sample 2, SDAS = 100 μm, magnification 50-times

Slika 12: Mikrostruktura modelne zlitine Al-w(Cu) 4.5 %, vidna pod LM: a) vzorec 1, SDAS = 83 μm in b) vzorec 2, SDAS = 100 μm, povečava 50-kratna

solidification with different SDAS in the range between 500 μm and 35 μm, and, actually this was obtained. **Figure 12** shows a typical dendrite morphology of the solidification formed during the alloy synthesis. **Figure 13** shows this microstructure visible under the SEM at different magnifications. At the highest magnification

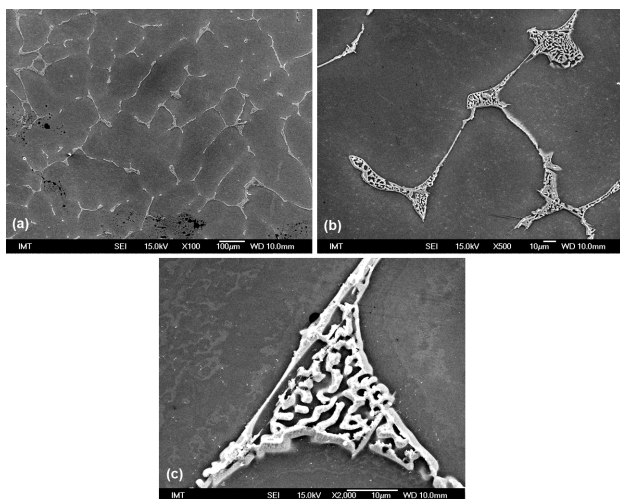
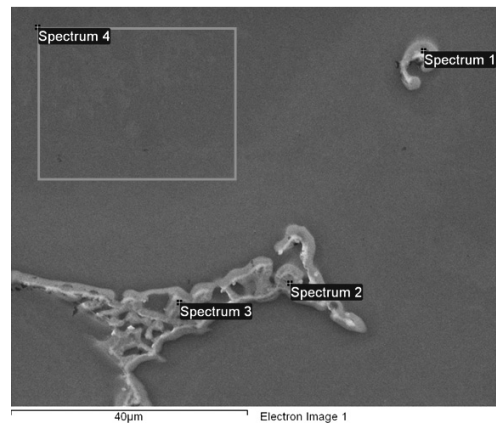


Figure 13: SE images of microstructure of model alloy Al-w(Cu) 4.5 % at different magnifications; sample 1: a) magnification 100-times, b) magnification 500-times and c) magnification 2000-times

Slika 13: SE-posnetki mikrostrukture modelne zlitine Al-w(Cu) 4.5 %, vzorec 1: a) povečava 100-kratna, b) povečava 500-kratna in c) 2000-kratna



Spectrum	O	Al	Ni	Cu
Spectrum 1	4.37	67.29		28.34
Spectrum 2	4.01	68.25		27.74
Spectrum 3	5.23	65.72	0.58	28.47
Spectrum 4		99.03		0.97

Figure 14: Area (metal matrix of α-Al solid solution) and point SEM/EDS analyses (secondary phase) of model alloy Al-w(Cu) 4.5 %
Slika 14: Ploskovna (kovinska matrica α-Al) in točkovna (sekundarna faza) SEM/EDS modelne zlitine Al-w(Cu) 4,5 %

one can clearly see the micro-chemical segregation due to non-equilibrium solidification.

Microchemical point, profile and EDS mapping were performed at different locations on the samples in order to obtain information about the local microchemical composition and the alloy segregation. **Figure 14** shows an example of point (Spectrums 1, 2 and 3) and mapping (Spectrum 4) EDS analyses. One can clearly see that in the interdendritic regions a secondary Al₂Cu phase, as well as Al₂O₃ oxide based is formed. It could be anticipated that the oxide inclusions are the nuclei for a secondary phase precipitation. **Figure 15** shows an example of profile analyses across the dendrite region. It is clear that the Cu-rich secondary phase has approximately

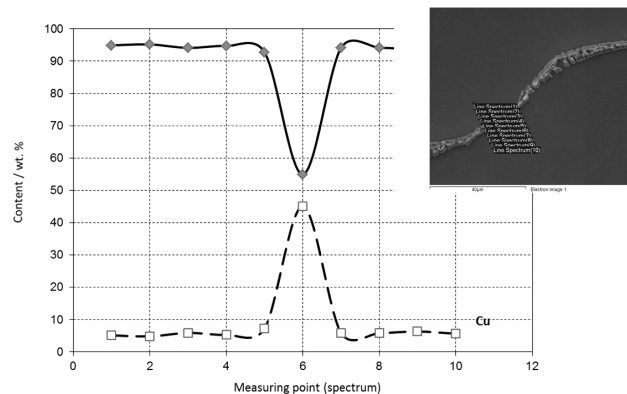


Figure 15: EDS profile analysis from Al metal matrix across secondary phase back to the metal matrix; Al and Cu concentration distribution

Slika 15: EDS profilna analiza iz kovinske α-Al osnove preko sekundarne faze in nazaj v kovinsko osnovo; porazdelitev koncentracije Al in Cu

$w(\text{Cu}) = 44 \%$, but the metal matrix, i.e., the $\alpha\text{-Al}$ solid solution, has approximately $w(\text{Cu}) = 5 \%$.

Non-continuous profile (10-points per $20 \mu\text{m}$) SEM/EDS analyses of metallographic samples cooled down with an average cooling rate of $10\text{--}12 \text{ }^\circ\text{C}/\text{min}$ have shown that four typical concentration profiles exist:

Generally, the concentration of Al continuously falls to a minimum crossing the secondary phase in the interdendritic regions (dendrite pockets) and then again the Al concentration increases back to the Al-based metal matrix. Simultaneously, the concentration of Cu changes in the opposite direction (Figure 15). The average local microchemical composition of the Al matrix is approximately $w = 95 \%$ Al and $w = 5 \%$ of Cu (amount fractions $\varphi = 97.7 \%$ Al and 2.3% of Cu) and the average local microchemical composition of the secondary phase is approximately $w = 56 \%$ of Al and 44% Cu ($\varphi = 75 \%$ Al and 25% of Cu). Theoretically, the metal matrix $\alpha\text{-Al}$ solid solution contains $w = 100 \%$ of Al at room temperature and approximately $\varphi = 98 \%$ Al and 2% Cu at $550 \text{ }^\circ\text{C}$. The secondary phase Al_2Cu contains theoretically at room temperature $\varphi = 66.7 \%$ of Al and 33.3% of Cu up to 68% of Al and 32% of Cu at $550 \text{ }^\circ\text{C}$. The experimentally determined composition is close to the equilibrium composition theoretically predicted at approximately $550 \text{ }^\circ\text{C}$. This is a consequence of the non-equilibrium solidification and the metastable condition of the model alloy at room temperature. It also has to be noted that the EDS information comes from a depth of about $1 \mu\text{m}$ to $3 \mu\text{m}$. The size and shape of this interaction volume is dependent on the primary beam energy and the sample material (Figure 16). For the surface analysis EDS is not the proper analytical method. In the case of very thin secondary phases, inclusions and surface analyses one must use a surface-sensitive analytical method such as Auger Electron Spectroscopy (AES).

Theoretical thermodynamic analyses predict the existence of some intermetallic phases ($\text{Al}_7\text{Cu}_2\text{Fe}$, $\text{Al}_7\text{Cu}_4\text{Ni}$, AlFeSi and crystals of Si) because of the presence of Fe,

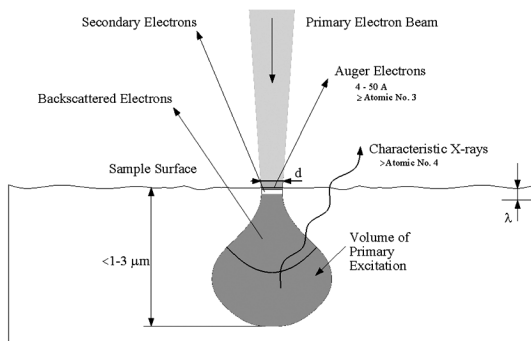


Figure 16: The interaction between an incident electron beam and the solid sample, showing the analysis volumes for Auger, secondary electrons, back scattered electrons and X-ray fluorescence

Slika 16: Interakcija vpadnega elektronskega curka s površino trdnega vzorca prikazuje analizni volumen za Augerjeve elektrone, sekundarne elektrone, povratno sipane elektrone in rentgensko fluorescenco

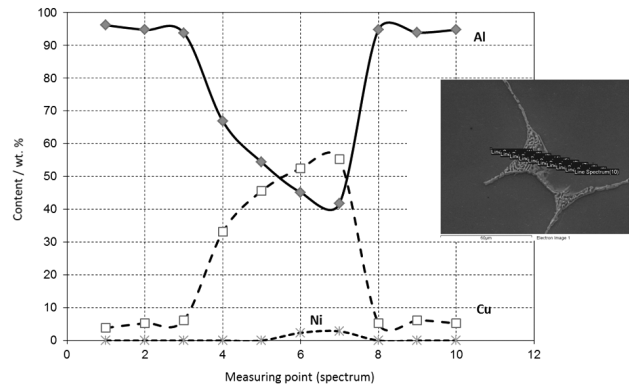


Figure 17: EDS profile analysis across $\alpha\text{-Al}$ dendrite region into the inter-dendritic region and back into the metal matrix; concentration distribution of Al, Cu and Ni

Slika 17: EDS profilna analiza iz kovinske $\alpha\text{-Al}$ osnove preko sekundarne faze in nazaj v kovinsko osnovo; porazdelitev koncentracije Al, Cu in Ni

Si and Ni in the investigated model alloy. Actually, at some places inside the secondary Al_2Cu phase we detected the presence of these elements. In the middle of the secondary phase, where the concentration of Cu is the highest, the EDS analyser detected small concentrations of Ni (Figure 17). The intermetallic phase

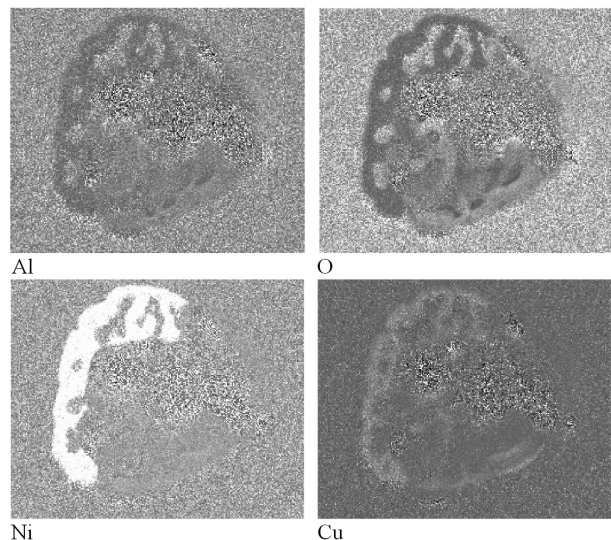
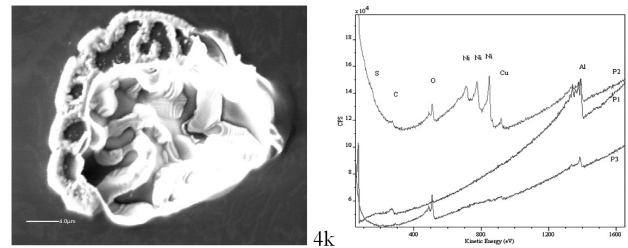


Figure 18: AES mapping of a precipitate of secondary phase in the model alloy Al-w(Cu) 4.5 % (sample 2) showing the distribution of selected elements Al, O, Ni and Cu and a clearly visible increased concentration of Ni

Slika 18: AES-mikroskopija porazdelitve izbranih elementov Al, O, Ni in Cu v izločku sekundarne faze v modelni zlitini Al-w(Cu) 4,5 % (vzorec 2) z dobro vidnim področjem povečane koncentracijo Ni

Al₇Cu₄Ni is stable from room temperature up to 550 °C and theoretically contains mass fractions $w = 51 \% \text{ Cu}$, $38 \% \text{ Al}$ and $11 \% \text{ of Ni}$. The EDS analyses give a lower Ni concentration ($w = 1.5 \% \text{ to } 3.5 \%$). However, the ratio $\text{Cu} : \text{Al}$ ($58 \% \text{ Cu} : 40 \% \text{ Al}$) perhaps confirms that at these places the Al₇Cu₄Ni phase or its non-equilibrium approximate is present. Therefore, we also performed SEM/AES analyses which suggest that at some places there is a higher local concentration of Ni (Figure 18). GIXRD (Grazing incidence X-Ray Diffraction) can help in the exact identification of the presence of this phase. However, this investigation was not planned in the frame of the project. It will be performed later and published elsewhere.

Aluminium has a high affinity for oxygen; therefore, it was expected that a slight oxidation of the alloy could happen during its synthesis. The SEM/EDS microanalyses have shown the presence of oxygen at some locations at the interdendritic locations. Figure 19 shows the profile EDS analysis across the secondary phase. The presence of a $x\text{SiO}_2 \cdot y\text{Al}_2\text{O}_3$ -based inclusion is clearly visible at the edge of it.

At some locations only Al₂O₃ is present. A proof of this is the simultaneous increased concentration of Al at these locations (Figure 20).

Finally, EDS analyses have also shown that practically all the elements of impurities are present at some locations in the interdendritic regions (Figure 21). This is important from the mechanical properties point of view because hard intermetallic phases in the interdendritic locations worsen the cohesive strength between the metal matrix and the interdendritic phase. Additionally, segregations are more extensive and the SDAS is larger, respectively, if the cooling rate is lower.

Figure 22 shows the average SDAS measured on samples 0, 1 and 2. The performed SDAS measurements

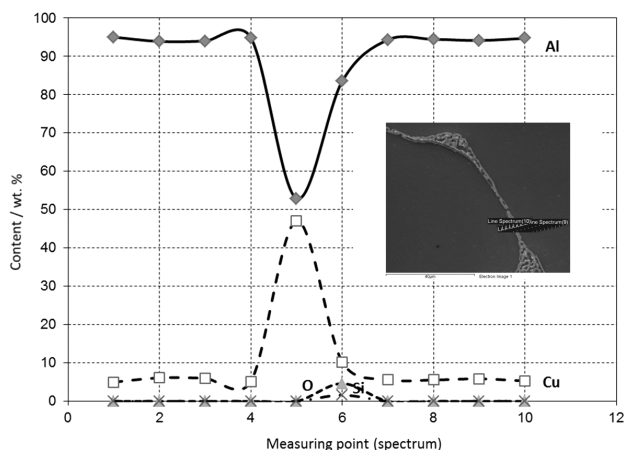


Figure 19: EDS profile analysis across α -Al dendrite region into the inter-dendritic region and back into the metal matrix; concentration distribution of Al, Cu, Si and O

Slika 19: EDS profilna analiza iz kovinske α -Al osnove preko sekundarne faze in nazaj v kovinsko osnovo; porazdelitev koncentracije Al, Cu, Si in O

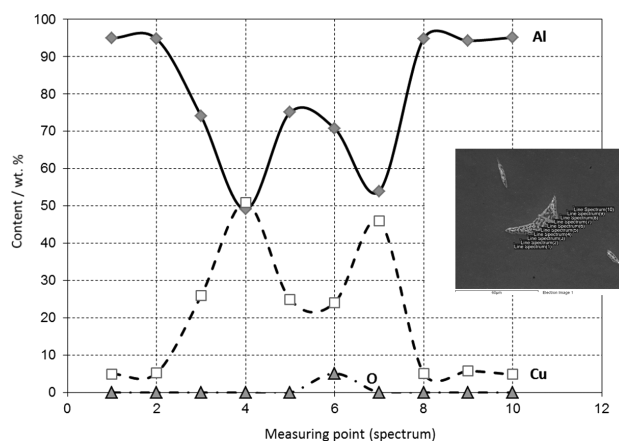


Figure 20: EDS profile analysis across α -Al dendrite region into the inter-dendritic region and back into the metal matrix; concentration distribution of Al, Cu and O

Slika 20: EDS profilna analiza iz kovinske α -Al osnove preko sekundarne faze in nazaj v kovinsko osnovo; porazdelitev koncentracije Al, Cu in O

show a relatively larger scatter of measured values from location to location. No evident law or regular change in SDAS as expected; for example, from the surface to the middle of the sample. The average measured values are between 79 μm and 110 μm , which corresponds to the theoretical initial cooling rate between 1.0 °C/s and approximately 2.5 °C/s (from 60 °C/min to 150 °C/min.). These cooling rates are higher than determined during the experiment (20–30 °C/min) at the thermocouple location. Besides, the thermocouple was isolated with an alumina tube against the effects of the melt. Therefore, further experimental work has to be considerably improved. In particular, the techniques of cooling-rate detection during solidification (smaller sample, larger number of thermocouples at different locations,

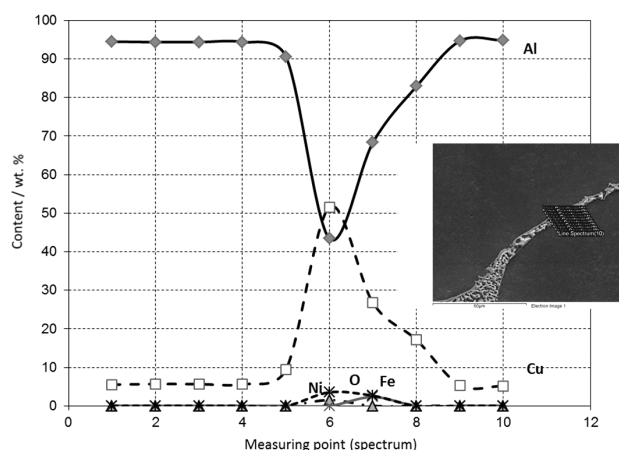


Figure 21: EDS profile analysis across α -Al dendrite region into the inter-dendritic region and back into the metal matrix; concentration distribution of Al, Cu, Fe, Ni and O

Slika 21: EDS profilna analiza iz kovinske α -Al osnove preko sekundarne faze in nazaj v kovinsko osnovo; porazdelitev koncentracije Al, Cu, Fe, Ni in O

Sample 0:

0_zg_L			0_zg_D		
79.1	94.4	90.6	81.8	98.6	107.9
87.8	89.2	79.0	89.4	91.3	84.0
67.0	90.5	97.8	92.8	90.1	93.3
83.8	82.3	103.9	95.2	81.6	76.3
83.1	87.5	88.6	88.5	79.0	76.4
100.4	102.6	94.5	102.1	108.2	87.7

0_sp_L 0_sp_D

Sample 1:

1_zg_L			1_zg_D		
96.8	79.2	98.8	86.9	98.7	84.0
104.7	114.2	85.9	69.4	84.1	94.7
90.5	83.9	72.2	90.8	84.9	95.4
87.6	126.0	79.5	87.3	107.2	76.3
71.8	100.4	87.1	96.1	119.0	98.0
87.1	95.2	105.5	83.5	92.2	97.7

1_sp_L 1_sp_D

Sample 3:

3_zg_L			3_zg_D		
106.9	99.7	100.2	89.9	77.5	92.3
98.8	97.7	112.6	94.5	69.9	99.4
92.2	77.1	99.3	84.5	91.4	97.3
94.3	104.7	86.4	90.8	86.5	106.4
109.8	90.3	95.4	104.4	100.8	89.0
100.5	93.2	99.2	110.0	91.0	94.4

3_sp_L 3_sp_D

Figure 22: Average *SDAS* measured in micrometers, measured on metallographic LM snapshots on individual samples cooled with different average cooling rates, in accordance with **Figure 11**

Slika 22: Povprečna velikost *SDAS* v mikrometrih, izmerjena na metalografskih LM-posnetkih na posameznih vzorcih, ohlajanih z različno povprečno hitrostjo; vezano na **slika 11**

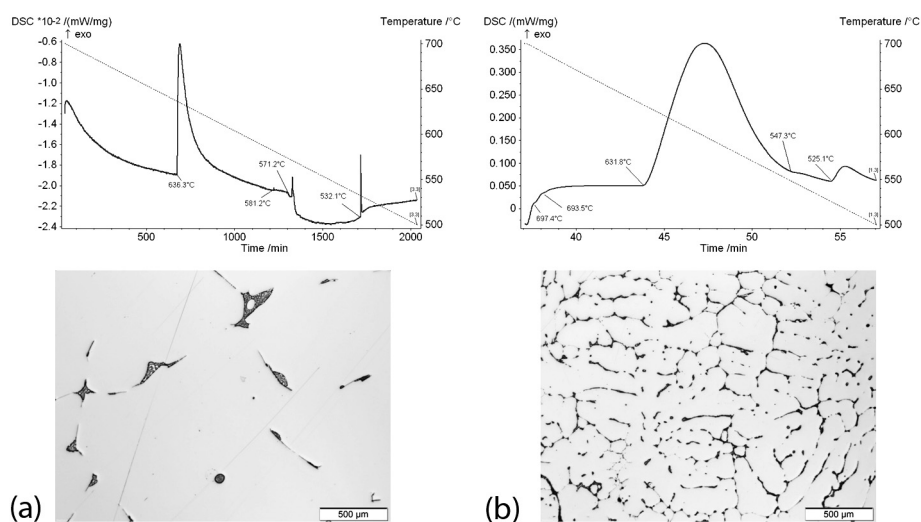


Figure 23: DSC cooling curves of model alloy Al-w(Cu) 4.5 %, cooled in the temperature region between 700 °C and 500 °C with two different cooling rates: a) 0.1 °C/min (*SDAS* > 700 μm) and b) 10 °C/min (*SDAS* ≈ 100 μm), with appropriate microstructural characteristics visible by LM.

Slika 23: DSC ohlajevalna krivulja modelne zlitine Al-w(Cu) 4,5 %, ohlajane v temperaturnem območju med 700 °C in 500 °C s hitrostjo: a) 0,1 °C/min (*SDAS* > 700 μm) in b) 10 °C/min (*SDAS* ≈ 100 μm), s pripadajočimi mikrostrukturnimi značilnostmi, vidnimi s svetlobnim mikroskopom

appropriate melting furnace etc.) must be additionally improved.

The most important for the formation of the solidification microstructure is the initial cooling rate and the cooling rate in the mushy zone, respectively. In the case of our model alloy the solidification interval is rather narrow and it is very difficult to control the solidification process on the relatively large samples that were initially selected. At the beginning of our experimental work we did not have enough experiences in the field. However, we became acquainted with the problems and gained a lot of experience in the field during the execution of the present project. In the late phase of the project we performed much more controlled cooling experiments in the DSC/TG apparatus (Netzsch STA 449C Jupiter) with smaller samples (ϕ 4.5 mm \times 5 mm, $m \approx 0.2$ g) and much more controlled cooling rates in the mushy zone. However, this equipment does not allow us to perform the experiments with very high cooling rates. Therefore, the selected cooling rates were (0.1, 0.5, 1.0, 10 and 25) °C/min. The DSC cooling curves show a big difference in solidification and phase precipitation, respectively, if the cooling rate is changed. A very clear and sharp phase formation is noticed at the lowest cooling rate (**Figure 23**). Details of these experiments will be published elsewhere separately, because of the limited space here.

4 CONCLUSIONS

Samples of the model alloy Al-w(Cu) 4.5 % with a controlled microstructure obtained at different cooling rates were synthesized in the frame of the present investigation. The obtained average cooling rates on larger samples (**Figure 6**) in the temperature interval from 600 °C to 200 °C are estimated to be 0.1 °C/min,

12 °C/min. and 1 220 °C/min. The size of the *SDAS* is controlled by the initial cooling rate and the cooling rate in the mushy zone, respectively. This cooling rate was estimated to be approximately 0.7 °C to 30 °C/min in the case of natural cooling and very slow cooling in the furnace. It is a rather larger cooling rate than the average measured cooling rate in the middle of the samples. The average measured *SDAS* on all the samples are between approximately 79 µm and 110 µm. This corresponds to the theoretical initial cooling rate of approximately between 1.0 °C/s and 2.5 °C/s. The only exception is the sample with the lowest selected average cooling rate (approx. 0.002 °C/s). In this case the *SDAS* was assessed to be more than 700 µm. But it was difficult to measure because even the lowest magnification (50-times) of the LM does not enable exact measurements. For this case much lower magnifications (10- to 25-times) are necessary. The performed investigations showed that more exact measurements of the cooling/solidification rate, especially in the mushy zone, are necessary. The experiments performed on smaller samples in the DSC/TG apparatus enabled better control of the solidification, but in a limited range (from 0.1 °C/min to 25 °C/min) of cooling rates. Therefore, new lab equipment (furnace) with a controllable atmosphere and accurate temperature control over a wider range of cooling rates (0.1–100 °C/s) for relatively small samples must be developed or purchased, respectively.

The next step of the performed investigations was the preparation of metallographic samples, as well as microstructural and microchemical investigations under the LM and SEM combined with EDS and AES microanalyses. The aim of these investigations was a determination of the segregation at the macro and micro levels, depending on the cooling rate of the synthesized model alloy. The microstructural composition of the naturally cooled model alloy is markedly in the non-equilibrium state, and similar to those predicted theoretically at 550 °C. Four characteristic states of chemical composition

are detected in the interdendritic regions because of the presence of impurities (Fe, Si, Ni) in the model alloy, as well as its slight oxidation during synthesis. For the synthesis and study of the pure binary Al-w(Cu) 4.5 %, model alloy it is necessary to select completely pure raw materials. Impurities can disturb some of the investigations to a certain extent. However, on the other hand, it can also help in understanding the complexity of multicomponent alloying systems.

Acknowledgement

The authors wish to thank the Slovenian Research Agency for financial support in the frame of project no.: J2-4120 and P2-0132, and to Professor Jožef Medved, Department for Metallurgy and Materials, University of Ljubljana, for assistance with the DSC/TG experiments.

5 REFERENCES

- ¹ Software package for thermodynamic calculations: Thermocalc; internet address: <http://www.thermo-calc.com/start/>
- ² U. R. Kattner: Thermodynamic Modelling of Multicomponent Phase Equilibria, *JOM*, 49 (1997) 12, 14–19
- ³ TAPP – Thermochemical and Physical Properties, A computer database, 1994
- ⁴ E. A. Brandes, G. B. Brook, *Smithells Metals Reference Book*, 7th Edition, Butterworth Heinemann Ltd., Oxford UK 199
- ⁵ J. F. Chinella, Z. Guo, Computational Thermodynamics Characterization of 7075, 7039, and 7020 Aluminum Alloys Using JMatPro, ARL, MD, USA, 2011
- ⁶ Z. Guo, N. Saunders, A. P. Miodownik, J. P. Schillé, Prediction of room temperature mechanical properties in aluminium castings, Proceedings of the 7th Pacific Rim International Conference on Modeling of Casting and Solidification Processes, Dalian, China, 2007
- ⁷ D. Hanumantha Rao, G. R. N. Tagore, G. Ranga Janardhana, Evolution of Artificial Neural Network (ANN) model for predicting secondary dendrite arm spacing in aluminium alloy casting, *J. Braz. Soc. Mech. Sci. & Eng.*, 32 (2010) 3, 276–281
- ⁸ B. Šarler et al., Advanced modelling and simulation of liquid-solid state processes, small basic project J2-4120, Slovenian Research Agency, internal reports, 2010–2013